Unlocking deep-trap data: Photonically engineered trap transfer strategy for secure phosphor memory

Lu Chen, Bingbing Yang, and Feng Liu*

State Key Laboratory of Integrated Optoelectronics, Key Laboratory of UV-Emitting Materials and Technology of Ministry of Education, School of Physics, Northeast Normal University, Changchun 130024, China

(Received 26 March 2026; accepted 10 August 2026; published 24 August 2026)

Secure, repeatable access to information stored in deep electron traps remains the central barrier to realizing the full potential of electron-trapping phosphors in next-generation optical memory. Existing readout methods typically rely on destructive thermal or nonselective optical stimulation, which limits repeated access and compromises data integrity. Here, we introduce photonically engineered trap transfer (PETT), a heat-free, nonvolatile approach enabling selective data extraction from deep traps. A specially designed garnet phosphor, $Gd_3Ga_5O_{12}$ codoped with Cr^{3+} and Eu^{3+}, serves as the storage medium, with Cr^{3+} acting as the luminescent center and Eu^{3+} engineering a hierarchical trap landscape. Data writing is achieved through an up-conversion charging process that embeds data within 0.01 s. In the PETT readout, visible light transfers electrons from deep to shallow traps; subsequent infrared stimulation releases them, producing a detectable luminescence signal. Kinetic modeling of the PETT process describes the time evolution of the shallow-trap population and reveals its characteristic rise-and-decay behavior. This method provides a reliable, selective, and repeatable route to data retrieval and establishes a robust physical framework for secure, multilevel, rewritable optical memory.

DOI: 10.1103/ym96-4sch

I. INTRODUCTION

In pursuit of advanced data storage solutions, optical storage technologies have gained prominence for their ability to encode and retrieve information using light, offering high storage densities, exceptional durability, and low energy consumption compared to conventional magnetic or electronic methods [1–5]. Within this domain, phosphor-based optical memory has emerged as a promising frontier by leveraging the luminescence properties of electron-trapping phosphors—materials that capture excitation energy in intrinsic traps and release it as light upon controlled stimulation [6–8]. This capability makes them well suited for nonvolatile memory systems that retain data over extended periods [9–13]. However, a critical challenge has persisted: Although these phosphors can securely "lock" data in stable deep traps for long periods [9–13], retrieving this information has traditionally required destructive thermal stimulation, thereby compromising data integrity and repeated access.

Current readout techniques highlight this fundamental trade-off [7–13]. Conventional optically stimulated luminescence (OSL) is heat-free but typically uses infrared light that lacks the selectivity needed to target stable deep traps. Visible-light stimulation offers an alternative [14–16], yet achieving clear spectral separation in visible-light-excitable materials remains difficult. To address this limitation, photostimulated persistent luminescence (PSPL) was developed to transfer electrons from deep to shallow traps [17–20]. However, PSPL relies on spontaneous afterglow that decays over time, preventing selective, delayed, or on-demand readouts.

To overcome these limitations, we propose an enhanced method, photonically engineered trap transfer (PETT). This approach integrates elements of OSL with PSPL through a controlled two-stage optical stimulation process. After initially relocating charges from deep to shallow traps with visible light, PETT employs an orthogonal infrared-stimulation step to redistribute electrons into shallower traps, enabling precise, on-demand readout of the luminescent signal via an infrared trigger (Fig. 1). This programmable manipulation enables precise control of signal timing and adjustable delays, ultimately improving the accuracy and versatility of optical data storage systems.

In this work, we demonstrate PETT using a tailored phosphor platform composed of $Gd_3Ga_5O_{12}$ codoped with Cr^{3+} and Eu^{3+}, where Cr^{3+} serves as the luminescent center and Eu^{3+} engineers a hierarchical trap landscape. Experiments reveal multiple nondestructive retrievals from a single 0.01 s write event, with data retention over months. Kinetic analysis of the PETT process quantitatively describes the electron-transfer dynamics, confirming the model's predictive power and providing clear guidelines for optimizing illumination parameters. These advances establish PETT as a versatile platform for secure, multilevel, rewritable optical memory.

II. METHODS

A. Sample preparation

To validate PETT, a series of garnet phosphors with compositions $Gd_3Ga_5O_{12}$:0.5% Cr^{3+}, x% Eu^{3+} ($x = 0$–5) was

*Contact author: fengliu@nenu.edu.cn

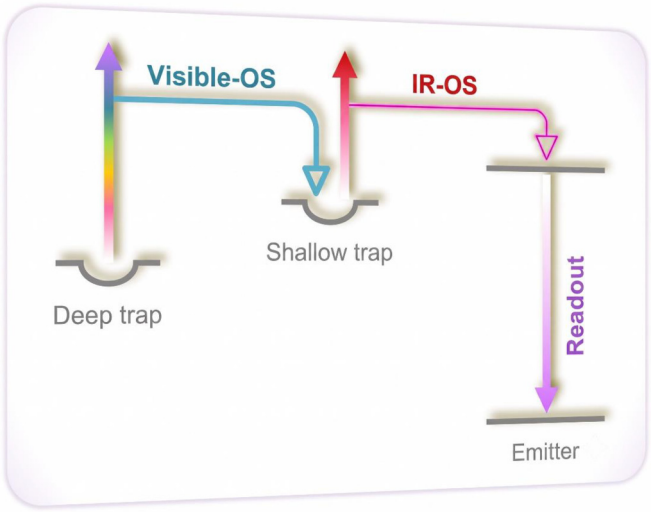

FIG. 1. PETT process in electron-trapping phosphors. Two-step optical stimulation involves visible-light irradiation to transfer electrons from deep to shallow traps, followed by infrared stimulation (IR-OS) to liberate electrons from shallow traps, resulting in selective luminescence readout.

synthesized via a conventional solid-state method. The raw powders used included Gd_2O_3 (99.99%, Alfa Aesar), Ga_2O_3 (99.999%, Aladdin), Cr_2O_3 (99.95%, Alfa Aesar), and Eu_2O_3 (99.99%, Alfa Aesar). These powders were thoroughly mixed and ground at room temperature, and then sintered at 1330 °C for 3 h to produce the final phosphor samples. For this study, we focused on the composition $Gd_3Ga_5O_{12}$:0.5% Cr^{3+}, 1% Eu^{3+}, abbreviated GGG:Cr,Eu.

B. Characterization

During characterization, emission spectra were acquired using a PTI 8075-11 QuantaMaster spectrofluorometer and an Ocean Optics QEpro spectrometer. The phosphors were excited and charged using a 450 nm laser via up-conversion excitation and charging process. For photo-stimulation, various handheld lightemitting diode (LED) sources were employed, including a blue flashlight (AloneFire E17, 5 W), a red flashlight (Darkness Beam UF1900, 3 W), an 850 nm infrared flashlight (UniqueFire T50, 5 W), a 940 nm infrared flashlight (UniqueFire T67, 10 W), and a high-power white LED flashlight (Ledlenser MT18). For optically stimulated luminescence using the 940 nm flashlight, the illumination reached the phosphor, which was filtered by a 790 nm short-pass filter (TSP01-790/SP, Semrock). Spectra were corrected for system responses and filter transmissions. Illumination intensities were measured using an illuminance meter (T-10A, Konica Minolta) and an optical power meter (PM320E, Thorlabs). Thermoluminescence curves were recorded using a TL Reader (Rongfan SL08-L) at a heating rate of 4 °C s^{-1}. Glow imaging was performed using a custom-built laser direct-writing system that transferred programmed data onto phosphor plates. A 450 nm fiber-coupled laser facilitated this process with an approximately 80 μm spot size and was mounted on a three-dimensional (3D) XYZ stage, enabling precise afterglow resolution. Images were captured at predetermined temperatures, with the sample held steady at each temperature throughout the exposure period to ensure consistent and accurate imaging conditions.

III. RESULTS AND DISCUSSION

A. Engineering shallow and deep traps

To investigate the potential of PETT in optical data storage, we selected a $Gd_3Ga_5O_{12}$ garnet host codoped with Cr^{3+} and Eu^{3+} ions. Previous studies have established the exceptional luminescence characteristics of Cr^{3+}-doped $Gd_3Ga_5O_{12}$, notably its extended afterglow emission at room temperature following ultraviolet excitation [21–23]. Building on this, we investigated the effects of lanthanide codoping, focusing on GGG:Cr,Eu. X-ray diffraction analysis confirmed the phase purity and cubic garnet structure of the codoped phosphor, consistent with the standard $Gd_3Ga_5O_{12}$ pattern (Fig. S1 in the Supplemental Material [24]).

Following ultraviolet excitation, GGG:Cr,Eu exhibited afterglow emission with a dominant peak at 720 nm, attributed to the (Cr^{3+}) $^2E/^4T_2 \rightarrow {}^4A_2$ transition. Upon illumination with a filtered xenon lamp, this afterglow occurs exclusively under short-wavelength irradiation (Fig. S2 in the Supplemental Material [24]), indicating that high-energy photons are required to ionize Cr^{3+} ions and initiate electron transfer to traps, as evidenced by the afterglow excitation spectrum [Fig. 2(a)] [25,26]. Additionally, the long-lived (Cr^{3+}) ^2E excited state enables up-conversion charging (UCC), in which visible or infrared light populates traps through a two-step ionization process [Fig. 2(a)] [27–30]. In a typical UCC process, intense illumination induces nonlinear excitation, effectively filling the phosphor's traps (Fig. S3 in the Supplemental Material [24]). Specifically, when exposed to a 450 nm laser at a power density of 2 W cm^{-2}, Cr^{3+} ions are initially excited to the $^4T_1$ level and then relax to the metastable ^2E state. Absorption of a second photon ionizes Cr^{3+}, filling the traps and resulting in the characteristic afterglow emission [Fig. 2(b)]. Codoping with Eu^{3+} preserves the afterglow emission spectral profiles but significantly modifies the trap distribution [31–33]. Thermoluminescence measurements showed that GGG:Cr,Eu possesses additional shallow traps with lower activation energies compared to the Cr-only sample [see Fig. 2(c)]. That is, while GGG:Cr contains primarily deep traps, the introduction of Eu^{3+} enriches the trap landscape, adding new shallow traps and increasing the overall structural complexity of the trap profile [illustrated in Fig. 2(a) and detailed in Fig. S4 in the Supplemental Material [24]]. Such increased complexity could offer potential benefits for advanced optical data storage technologies.

To evaluate the data recording and retrieval performance, we conducted luminescence imaging experiments on both GGG:Cr,Eu, and GGG:Cr, as illustrated in the insets of Fig. 2(c). Using a 450 nm laser direct-writing system, we inscribed two patterns onto each phosphor: the "firewood" pattern at room temperature and the "flame" pattern at 220 °C. After irradiation ceased and the samples cooled to room temperature, GGG:Cr,Eu displayed a pronounced afterglow for the "firewood" pattern. In contrast, the afterglow from GGG:Cr was nearly undetectable, consistent with its thermoluminescence profile. Raising the temperature to

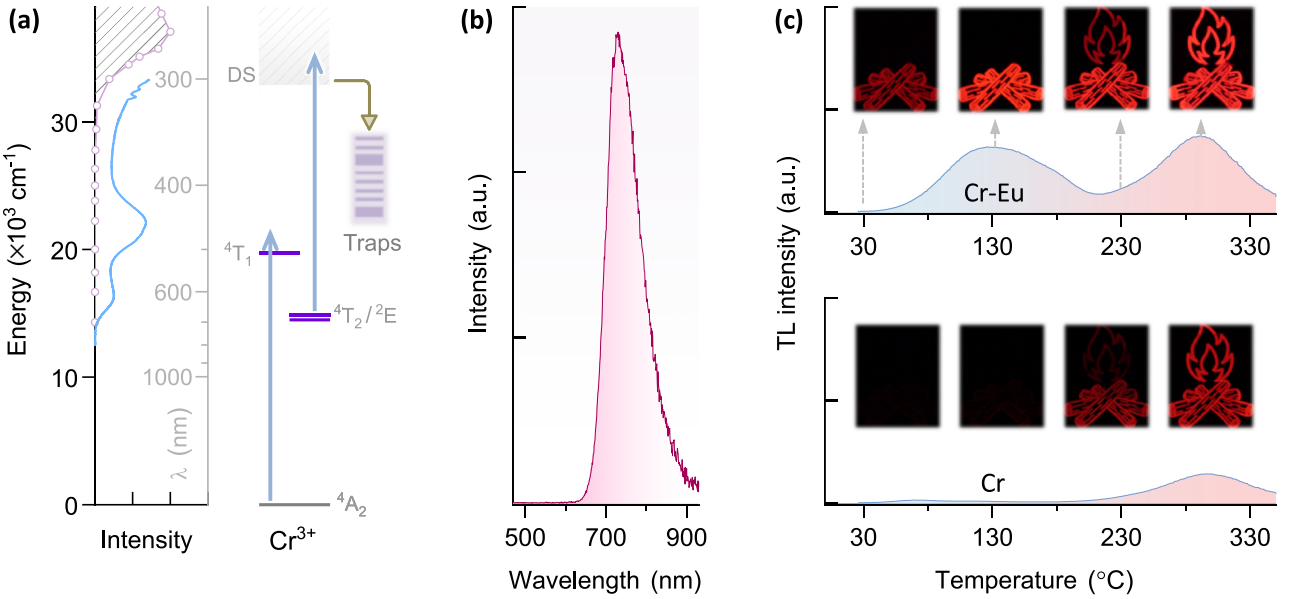

FIG. 2. Up-conversion charging and trap characterization of GGG:Cr,Eu. (a) Afterglow excitation spectrum (data points with connecting lines) and diffuse reflectance spectrum (solid line). To enhance clarity, the vertical axis presents both energy and wavelength scales. The right panel illustrates the UCC pathway and the complex trap landscape involved. (b) Afterglow emission spectrum recorded at room temperature following UCC upon exposure to a 450 nm laser. (c) Thermoluminescence curves of GGG:Cr,Eu and GGG:Cr following UCC. Insets show afterglow images of inscribed patterns (2 s exposure).

230 °C allowed both phosphors to reveal clear "firewood" and "flame" patterns over an area measuring 2 cm × 2.4 cm. These findings highlight the role of Eu^{3+} in tailoring trap distributions within the phosphor, enabling room-temperature afterglow in the codoped material and underscoring its potential for advanced optical storage applications.

B. Photonically engineered trap transfer for selective data access

In storage phosphors, luminescence behavior is governed by trap characteristics and their interaction with luminescent centers. In GGG:Cr,Eu, shallow traps release electrons gradually at room temperature, while deep traps preserve information reliably over prolonged periods. To access deep-trap data without external heating, optical stimulation techniques offer effective solutions [14–16]. Following UCC, we exposed the phosphor to various light sources, including a blue flashlight (5 W, 60 s), a red flashlight (3 W, 60 s), an 850 nm infrared flashlight (5 W, 60 s), and a 940 nm infrared flashlight (10 W), yielding distinct thermoluminescence depletion profiles [Fig. 3(a)]. Infrared stimulation (940 or 850 nm, 60 s) partially emptied shallow traps, whereas visible illumination (red or blue) depleted both shallow and deep traps, demonstrating wavelength-dependent selectivity. This selectivity supports the design and validation of the PETT model.

To validate PETT in GGG:Cr,Eu post-UCC, we first heated the phosphor to 220 °C to deplete the shallow traps, and then exposed it to blue flashlight illumination at a power density of 2 mW cm^{-2} for 60 s. This process facilitated the transfer of electrons from deep to shallow traps, repopulating the shallow traps and enabling subsequent infrared-stimulated readout [Fig. 3(b)], aligning with the two-stage PETT mechanism. Notably, initial heating is not strictly necessary; shallow traps can instead be gradually released at ambient temperature over an extended period (see Fig. S5 in the Supplemental Material [24]).

To illustrate the practical application of PETT, we designed a "digit puzzle" demonstration resembling a Sudoku grid, featuring "given clues" and "deduced numbers" [Fig. 3(c)]. We employed our 450 nm laser direct-writing system to inscribe the "deduced numbers" onto a GGG:Cr,Eu phosphor plate at room temperature, populating both trap types. Subsequent heating to 220 °C selectively depleted shallow traps, concealing the "deduced numbers" in deep traps. We then inscribed the "given clues" at room temperature. After 1 h in darkness, the room temperature afterglow faded. A 940 nm flashlight revealed the "given clues" via shallow-trap stimulation, leaving the "deduced numbers" in deep traps. Applying PETT—a blue flashlight exposure followed by 940 nm irradiation—transferred electrons from deep to shallow traps, retrieving the complete grid [Fig. 3(c)]. We further plotted the emission intensity of layered data over time following UCC, as shown in the lower part of Fig. 3(c). The two plotted curves quantitatively validate the imaging process, aligning with afterglow observations, and demonstrate PETT's capacity for selective, room-temperature data access, as well as its promise for hierarchical optical memory systems.

C. Electron-transfer dynamics in the PETT process

To quantitatively describe the PETT process, we developed a simplified kinetic model based on rate equations for a two-trap system [deep and shallow traps, Fig. 4(a)]. A defining

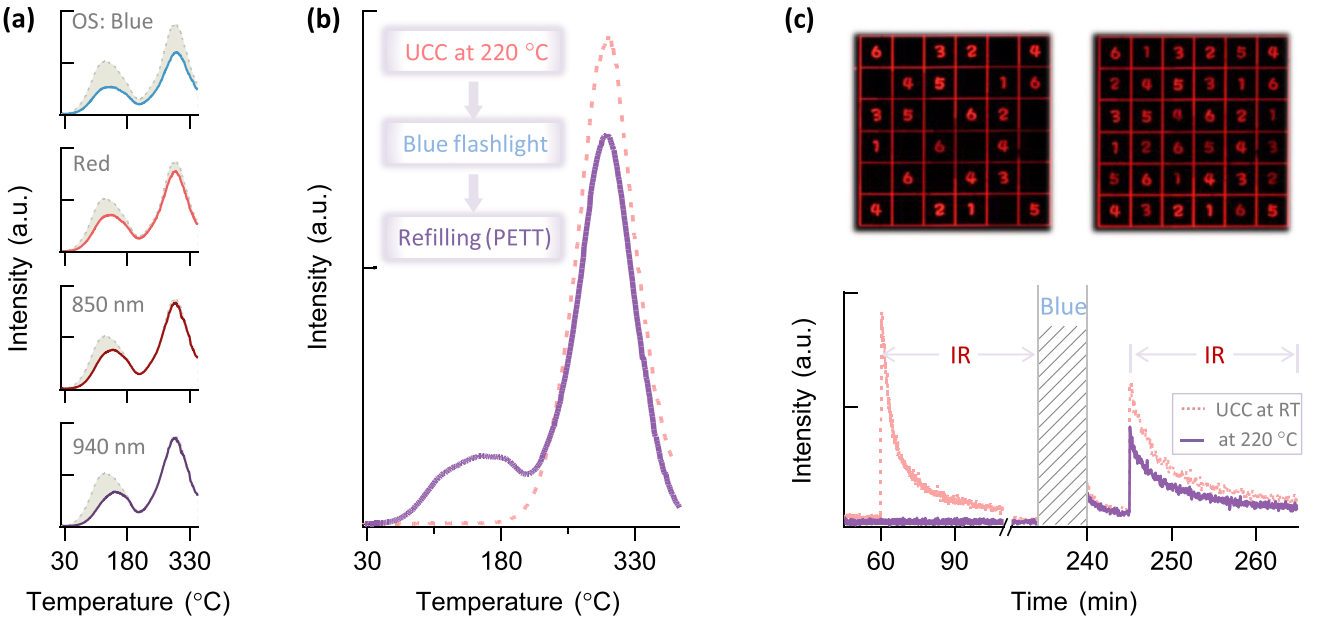

FIG. 3. Photonically engineered trap transfer in GGG:Cr,Eu phosphor. (a) Thermoluminescence profiles recorded under stimulations from different light sources: a blue flashlight, a red flashlight, an 850 nm infrared flashlight, and a 940 nm infrared flashlight. The shaded areas represent baseline curves without optical stimulation. (b) Thermoluminescence curves depicting electron transfer from deep to shallow traps upon blue-light exposure. UCC at 220 °C fills only deep traps (dashed line), whereas the illumination of a blue flashlight (2 mW cm^{-2}, 60 s) depletes deep traps and refills shallow ones (solid line). (c) Luminescence imaging of a "digit puzzle" grid, revealing selective retrieval of "given clues" and "deduced numbers" via sequential blue flashlight and 940 nm infrared stimulations. Each small grid measures 2 mm × 2 mm, with an imaging exposure time of 2 s. The bottom panel shows quantitative intensity profiles over time, confirming the sequential access to layered data.

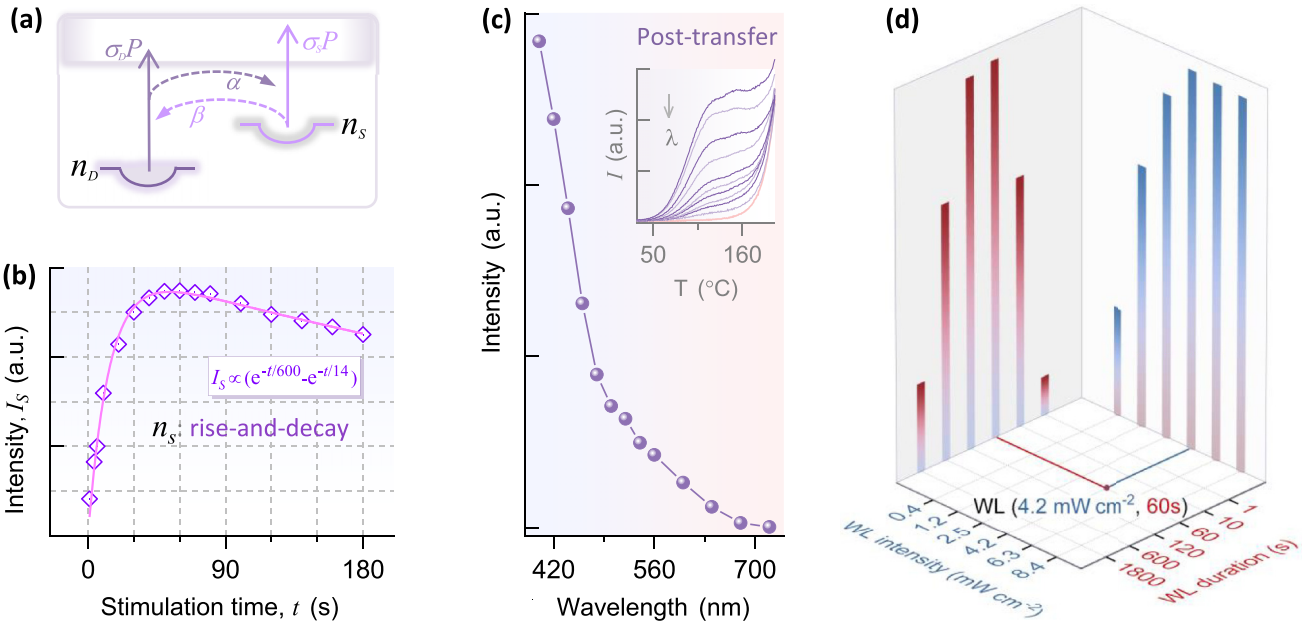

FIG. 4. Kinetic modeling and experimental characterization of the PETT process in GGG:Cr,Eu. (a) Schematic of the two-trap kinetic model illustrating visible-light-driven electron transfer between deep traps (population n_D) and shallow traps (n_S). (b) Integrated thermoluminescence intensity of the shallow-trap band vs blue-light illumination duration (2 mW cm^{-2}) after UCC and preheating. The solid line shows a biexponential fit, capturing the characteristic rise and decay of the shallow-trap population. (c) Wavelength dependence of shallow-trap repopulation. The inset shows thermoluminescence curves after 60 s monochromatic illumination. (d) Shallow-trap thermoluminescence intensity vs white-light power density (right) and illumination time at 4.2 mW cm^{-2} (left), identifying optimal PETT conditions.

feature of PETT is the visible-light-driven electron transfer from deep to shallow traps. We assume that all electrons initially reside in the deep traps with population n_D, while the shallow traps are initially empty ($n_S = 0$). Under illumination, electrons transfer from deep to shallow traps with a probability α and can return with probability β. When driven solely by visible-light exposure, the time evolution of the system is governed by the coupled rate equations:

$$\frac{dn_D}{dt} = -\sigma_D P n_D + \beta \sigma_S P n_S, \tag{1}$$

$$\frac{dn_S}{dt} = \alpha \sigma_D P n_D - \sigma_S P n_S. \tag{2}$$

Here, σ_D and σ_S represent the photoionization cross sections for the deep and shallow traps, respectively, and P is the stimulation-light power. The terms $\sigma_D P$ and $\sigma_S P$ denote the stimulated emptying rates for the respective traps.

To solve the coupled differential Equations (1) and (2), we employ an eigenvalue approach. The solution reveals that the temporal evolution of the shallow-trap population is described by the difference of two exponential components:

$$n_s = C(e^{-C_1 P t} - e^{-C_2 P t}). \tag{3}$$

In this expression, C, C_1, and C_2 are dimensionless constants determined by initial conditions and the system parameters σ_D, σ_S, α, and β (see Fig. S6 in the Supplemental Material [24]). In experimental scenarios, these constants are treated as fitting variables.

Equation (3) indicates that under consistent illumination, the shallow-trap population initially rises, reaches a maximum, and subsequently declines. This mathematical structure captures the essential dynamics of the PETT process driven by visible-light stimulation. To verify this behavior within the GGG:Cr,Eu system, we conducted thermoluminescence experiments following the protocol depicted in Fig. 3(b). The sample was first charged via UCC, heated to 220 °C to empty the shallow traps, and subsequently exposed to blue flashlight illumination (2 mW cm^{-2}) for varying durations (see Fig. S6 in the Supplemental Material [24]). We recorded the integrated intensity of the shallow-trap thermoluminescence band as a function of illumination duration to quantify transfer efficiency [refer to Fig. 4(b)]. Fitting the data with Eq. (3) revealed a clear biexponential trend, confirming that the rate-equation model accurately captures the PETT dynamics.

Besides illumination time, Eq. (3) also highlights how the wavelength composition and power of the stimulation light impact PETT behavior. To investigate these factors further, the GGG:Cr,Eu phosphor was first exposed to filtered xenon light spanning 400–720 nm (around 0.2 mW cm^{-2}) for 60 s after deep-trap charging and shallow-trap emptying. After each wavelength-specific illumination, we recorded the shallow-trap thermoluminescence intensity [see the inset of Fig. 4(c)]. Figure 4(c) illustrates how these intensities vary with illumination wavelength, with the data corrected for the xenon lamp's spectral distribution. The results show that shorter wavelengths are more effective at repopulating shallow traps, implying that broad-spectrum white light could be a practical tool for promoting trap transfer.

Subsequently, we explored how the stimulation-light intensity affects the PETT process by illuminating the GGG:Cr,Eu phosphor with white light at levels ranging from 0.4 to 8.4 mW cm^{-2} for 60 s (see Fig. S7 in the Supplemental Material [24]). The shallow-trap thermoluminescence intensity increased with the white-light power density, reaching a maximum at around 4.2 mW cm^{-2}, which corresponds to an illuminance of roughly 10 klx. Beyond this optimal point, further increases in power density yielded no additional thermoluminescence enhancement [Fig. 4(d), right]. The power-dependent behavior is also well described by Eq. (3); with the wavelength composition and exposure time held constant, the shallow-trap population across different power levels exhibits the expected biexponential profile (see Fig. S7 in the Supplemental Material [24]). Furthermore, maintaining a constant white-light power density (4.2 mW cm^{-2}) produced a maximum thermoluminescence intensity after 60 s of exposure [Fig. 4(d), left], aligning with model predictions.

These results demonstrate that the duration, wavelength composition, and illumination power are key tunable parameters for maximizing PETT efficiency in multitrap phosphors. The kinetic model thus provides both mechanistic insight and practical optimization guidelines for designing PETT-based optical memory systems.

D. Long-term stability and repeated readout using PETT

These findings highlight PETT's capacity for multilevel data storage. Leveraging this capability alongside the UCC performance of GGG:Cr,Eu, we realized multilevel optical memory using a 450 nm laser direct-writing system (100 mW per pixel, 0.01 s exposure). As illustrated in Fig. 5(a), we encoded three distinct datasets into traps of varying depths. We first recorded data 1 (D_1, firework pattern) onto the phosphor and heated it to 220 °C to ensure retention within the deep traps. Next, we inscribed data 2 (D_2, buildings) while elevating the sample temperature to 120 °C and storing this information in deep and medium-depth traps. Finally, we introduced data 3 (D_3, trees) into the traps at room temperature, completing the multilevel encoding process. It is important to clarify that D_1, D_2, and D_3 do not correspond to distinct trap species in this system. Given the broad thermoluminescence bands of GGG:Cr,Eu, and the practical requirements of multilevel storage, we subdivided the shallow-trap band into two effective layers for demonstration purposes—assigning D_2 and D_3 to these layers, with D_1 residing in the deep traps.

In the retrieval phase, we directly extracted information from the emission signal, as depicted in Fig. 5(b). Data 3 (D_3) emerged immediately at room temperature as an afterglow. After 2 days of storage in darkness, the afterglow diminished, yet we accessed data 2 and 3 ($D_2 + D_3$) via optical stimulation with the 940 nm infrared flashlight. Meanwhile, data 1 (D_1) remained latent within the deep traps. Following 20 days of dark storage, we exposed the sample to white light (4.2 mW cm^{-2}, 60 s). This white-light stimulation activated the PETT process, thereby transferring electrons from deep traps to refill shallow traps. Subsequent application of 940 nm infrared light revealed the previously hidden patterns as visible emissions, all displayed over an area of 4 cm ×

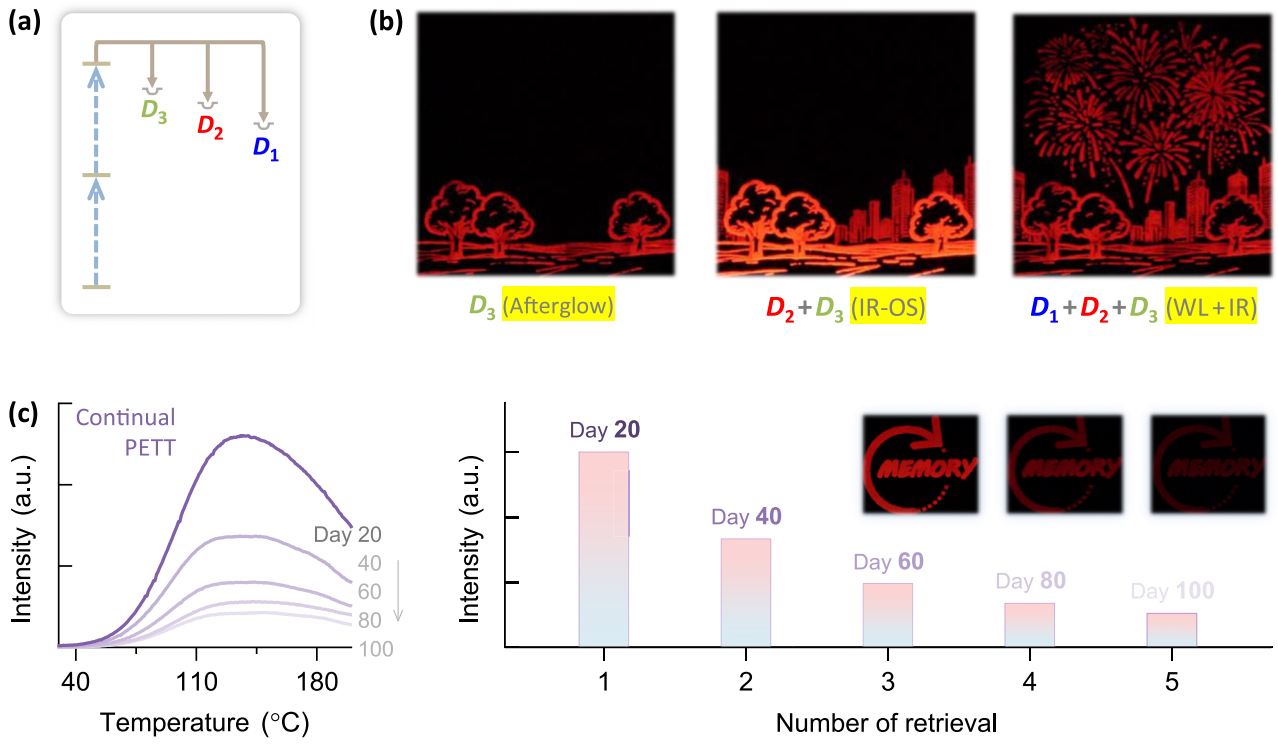

FIG. 5. Demonstration of PETT in GGG:Cr,Eu for hierarchical optical memory. (a) Data recording via UCC at varying trap depths: data 1 (firework pattern) in deep traps at 220 °C, data 2 (buildings) in deep and medium-depth traps at 120 °C, and data 3 (trees) in all traps at room temperature. (b) Luminescence imaging: immediate afterglow reveals data 3; after 2 days, 940 nm IR stimulation accesses data 2 and 3; after 20 days, PETT with white light (4.2 mW cm^{-2}, 60 s) followed by 940 nm IR stimulation retrieves data 1. (c) Thermoluminescence curves showing shallow-trap intensity measured every 20 days across multiple retrieval cycles, with ∼20% signal retention after 100 days (fifth read cycle), confirming PETT's capability for long-term, repeatable data retrieval. Insets show images captured at 20 days (first read cycle), 60 days (third read cycle), and 100 days (fifth read cycle), each with a 2 s exposure time.

4 cm. Quantitative emission intensity measurements over time under different stimulation conditions (refer to Fig. S8 in the Supplemental Material [24]) confirmed the layered retrieval method, highlighting the strong potential of this technique for encrypted data storage.

Moreover, the deep traps in GGG:Cr,Eu play a crucial role in supporting long-term data storage and facilitate continual retrieval of the stored information. To investigate the storage capacity and durability of the phosphor, we conducted thermoluminescence measurements at various delay intervals, as illustrated in Fig. 5(c). Specifically, following UCC and subsequent thermal emptying at 220 °C, we exposed the sample to white light (4.2 mW cm^{-2}, 60 s) and measured the shallow-trap thermoluminescence intensity (30–200 °C). This measurement indicates the degree of shallow-trap reoccupation. After storing the sample in a dark environment for 20 days, during which the shallow traps at room temperature were completely emptied, we re-exposed it to white light and recorded the shallow-trap thermoluminescence intensity again. We repeated this cycle every 20 days. Over 100 days, the shallow traps retained approximately 20% of the initial intensity, demonstrating PETT's capability for long-term data retention and repeated retrieval. Nonetheless, this performance shows a gradual decline in signal across cycles, indicating room for further optimization. Considering the observed cycle performance of PETT, we suggest distinct approaches tailored to specific application requirements: For scenarios requiring high data integrity, limiting reads to a single read is advisable, whereas for applications where some loss of fidelity is acceptable, performing 4–5 read cycles is feasible.

IV. CONCLUSIONS

We have developed photonically engineered trap transfer, a heat-free, nondestructive optical method for the selective and repeatable readout of data stored in deep electron traps. Using a $Gd_3Ga_5O_{12}$:Cr^{3+}, Eu^{3+} garnet platform, we show that a two-stage process—visible-light prestimulation followed by infrared readout—enables multiple nonvolatile retrievals from a single 0.01 s write operation, with data integrity preserved for months at room temperature. By decoupling trap filling from controlled electron redistribution, PETT overcomes key limitations of conventional OSL and PSPL methods, providing exceptional temporal control over luminescence signals. Our quantitative kinetic model successfully captures the electron-transfer dynamics and identifies the characteristic rise-and-decay profile, providing a predictive framework for optimizing illumination parameters. While the PETT principle can be adapted to other phosphors with hierarchical traps (Fig. S9 in the Supplemental Material [24]), further advancements in materials engineering and device integration remain

essential to improving storage density and read/write speed. These advances position PETT as a promising alternative for specialized optical memory applications.

ACKNOWLEDGMENTS

The authors thank Prof. Xiao-jun Wang from Georgia Southern University for his valuable insights into the trap-transfer dynamics. We also acknowledge Mina Liu, Zhirui Zhang, and Ziyi Wang from the High School Attached to Northeast Normal University for their dedicated efforts in preparing the supplementary samples. The work was supported by the National Natural Science Foundation of China (Grants No. 12574434, No. 52595642, and No. 52595640) and the Open Foundation of State Key Laboratory of Luminescent Materials and Devices (2025-skllmd-22).

DATA AVAILABILITY

The data that support the findings of this article are available on request from the authors.

[1] M. Gu, X. P. Li, and Y. Y. Cao, Optical storage arrays: A perspective for future big data storage, Light Sci. Appl. **3**, e177 (2014).

[2] D. A. Parthenopoulos and P. M. Rentzepis, Three-dimensional optical storage memory, Science **245**, 843 (1989).

[3] E. Walker and P. M. Rentzepis, A new dimension, Nat. Photon. **2**, 406 (2008).

[4] Z. R. Zhao, Z. J. Wang, Y. Y. Shi, S. Wan, and Z. Y. Li, Multidimensional-encrypted meta-optics storage empowered by diffraction-order decoupling, Adv. Mater. **37**, 2419322 (2025).

[5] M. Zhao, J. Wen, Q. Hu, X. B. Wei, Y. W. Zhong, H. Ruan, and M. Gu, A 3D nanoscale optical disk memory with petabit capacity, Nature (London) **626**, 772 (2024).

[6] S. Jutamulia, G. M. Storti, J. Lindmayer, and W. Seiderman, Use of electron trapping materials in optical signal processing. 1: Parallel Boolean logic, Appl. Opt. **29**, 4806 (1990).

[7] L. F. Yuan, Y. H. Jin, Y. Su, H. Y. Wu, Y. H. Hu, and S. H. Yang, Optically stimulated luminescence phosphors: Principles, applications, and prospects, Laser Photon. Rev. **14**, 2000123 (2020).

[8] Y. X. Zhuang, L. Wang, Y. Lv, T. L. Zhou, and R. J. Xie, Optical data storage and multicolor emission readout on flexible films using deep-trap persistent luminescence materials, Adv. Funct. Mater. **28**, 1705769 (2018).

[9] Z. H. Hu, J. Y. Guan, S. T. Zheng, Z. H. Chai, S. Z. Wu, D. Liu, J. Su, F. Z. Shi, C. K. Duan, Y. Wang, and K. W. Xia, Burn after read: A rewritable multiplexing optical information storage and encryption method, Laser Photon. Rev. **18**, 2301024 (2024).

[10] D. Liu, L. F. Yuan, Y. H. Jin, H. Y. Wu, Y. Lv, G. T. Xiong, G. F. Ju, L. Chen, S. H. Yang, and Y. H. Hu, Tailoring multidimensional traps for rewritable multilevel optical data storage, ACS Appl. Mater. Interfaces **11**, 35023 (2019).

[11] H. T. Tang, Z. C. Liu, H. Zhang, X. D. Zhu, Q. P. Peng, W. Wang, T. Ji, P. Zhang, Y. K. Le, A. N. Yakovlev, J. B. Qiu, G. P. Dong, X. Yu, and X. H. Xu, 4D optical information storage from $LiGa_5O_8$:Cr^{3+} nanocrystal in glass, Adv. Opt. Mater. **11**, 2300445 (2023).

[12] Y. Xie, Y. P. Song, G. T. Sun, P. F. Hu, A. Bednarkiewicz, and L. N. Sun, Lanthanide-doped heterostructured nanocomposites toward advanced optical anti-counterfeiting and information storage, Light Sci. Appl. **11**, 150 (2022).

[13] L. Chen, X. Q. Liu, F. Liu, C. Liao, L. L. Zhang, J. H. Zhang, X. J. Wang, and Y. C. Liu, Unlocking the potential of up-conversion charging for rapid and high-resolution optical storage with phosphors, Light Sci. Appl. **14**, 107 (2025).

[14] B. B. Yang, Z. C. Yu, X. Q. Liu, Y. Liu, F. Liu, H. Wu, J. H. Zhang, X. J. Wang, and Y. C. Liu, Photostimulated ultraviolet luminescence for anti-counterfeiting in daylight conditions, Laser Photon. Rev. **19**, 2401606 (2025).

[15] X. Y. Zhao, F. Liu, X. J. Wang, and Y. C. Liu, Emission from storage phosphors that glow even in bright ambient light, Phys. Rev. Appl. **15**, 064039 (2021).

[16] X. Y. Zhao, F. Liu, Z. C. Yu, X. Li, C. R. Wang, F. Chen, and X. J. Wang, Sunlight stimulated solar-blind ultraviolet phosphor, Phys. Rev. Res. **4**, L012028 (2022).

[17] F. Liu, W. Z. Yan, Y. J. Chuang, Z. P. Zhen, J. Xie, and Z. W. Pan, Photostimulated near-infrared persistent luminescence as a new optical read-out from Cr^{3+}-doped $LiGa_5O_8$, Sci. Rep. **3**, 1554 (2013).

[18] Y. J. Liang, F. Liu, Y. F. Chen, X. J. Wang, K. N. Sun, and Z. W. Pan, New function of the Yb^{3+} ion as an efficient emitter of persistent luminescence in the short-wave infrared, Light Sci. Appl. **5**, e16124 (2016).

[19] H. X. Sun, Q. Q. Gao, A. Y. Wang, Y. C. Liu, X. J. Wang, and F. Liu, Ultraviolet-B persistent luminescence and thermoluminescence of bismuth ion doped garnet phosphors, Opt. Mater. Express **10**, 1296 (2020).

[20] Y. N. Luan, Q. Sun, Y. Liu, T. X. Shi, F. Liu, L. L. Zhang, J. H. Zhang, X. J. Wang, and Y. C. Liu, Multi-level phosphor storage enabled by synergistic up-conversion and photostimulated trap manipulation, Commun. Mater. **6**, 155 (2025).

[21] J. Xu, J. Ueda, and S. Tanabe, Toward tunable and bright deep-red persistent luminescence of Cr^{3+} in garnets, J. Am. Ceram. Soc. **100**, 4033 (2017).

[22] U. Hommerich and K. L. Bray, High-pressure laser spectroscopy of Cr^{3+}:$Gd_3Sc_2Ga_3O_{12}$ and Cr^{3+}:$Gd_3Ga_5O_{12}$, Phys. Rev. B **51**, 12133 (1995).

[23] J. Pareja, C. Litterscheid, A. Molina, B. Albert, B. Kaiser, and A. Dreizler, Effects of doping concentration and co-doping with cerium on the luminescence properties of $Gd_3Ga_5O_{12}$:Cr^{3+} for thermometry applications, Opt. Mater. **47**, 338 (2015).

[24] See Supplemental Material at http://link.aps.org/supplemental/10.1103/ym96-4sch for Figs. S1−S9.

[25] Z. W. Pan, Y. Y. Lu, and F. Liu, Sunlight-activated long-persistent luminescence in the near-infrared from Cr^{3+}-doped zinc gallogermanates, Nat. Mater. **11**, 58 (2012).

[26] W. Z. Yan, F. Liu, Y. Y. Lu, and Z. W. Pan, Near infrared long-persistent phosphorescence in $La_3Ga_5GeO_{14}$:Cr^{3+} phosphor, Opt. Express **18**, 20215 (2010).

[27] F. Liu, Y. J. Liang, and Z. W. Pan, Detection of up-converted persistent luminescence in the near infrared emitted by $Zn_3Ga_2GeO_8:Cr^{3+}$, Yb^{3+}, Er^{3+} phosphor, Phys. Rev. Lett. **113**, 177401 (2014).

[28] F. Liu, Y. F. Chen, Y. J. Liang, and Z. W. Pan, Phonon-assisted upconversion charging in $Zn_3Ga_2GeO_8:Cr^{3+}$ near-infrared persistent phosphor, Opt. Lett. **41**, 954 (2016).

[29] S. Y. Yan, F. Liu, J. H. Zhang, X. J. Wang, and Y. C. Liu, Persistent emission of narrowband ultraviolet-B light upon blue-light illumination, Phys. Rev. Appl. **13**, 044051 (2020).

[30] X. Q. Liu, L. Chen, X. W. Huo, F. Liu, C. Liao, L. L. Zhang, J. H. Zhang, S. A. Zhang, Y. Li, X. J. Wang, and Y. C. Liu, From two-step excitation to persistent luminescence: Revisiting $ZnGa_2O_4:Cr^{3+}$ phosphor through upconversion charging approach, Adv. Opt. Mater. **12**, 2303018 (2024).

[31] F. T. You, A. J. J. Bos, Q. F. Shi, S. H. Huang, and P. Dorenbos, Thermoluminescence investigation of donor (Ce^{3+}, Pr^{3+}, Tb^{3+}) acceptor (Eu^{3+}, Yb^{3+}) pairs in $Y_3Al_5O_{12}$, Phys. Rev. B **85**, 115101 (2012).

[32] T. S. Lyu, P. Dorenbos, and Z. H. Wei, Designing $LiTaO_3:Ln^{3+}$, Eu^{3+} (Ln = Tb or Pr) perovskite dosimeter with excellent charge carrier storage capacity and stability for anti-counterfeiting and flexible X-ray imaging, Chem. Eng. J. **461**, 141685 (2023).

[33] T. X. Shi, F. Liu, Y. C. Liu, and X. J. Wang, Unveiling the influence of ambient lighting on stimulating ultraviolet luminescence of deep-trap phosphors, J. Appl. Phys. **135**, 083109 (2024).